NUCL SCI TECH (2018) 29:58
https://doi.org/10.1007/s41365-018-0397-x

Shielding effectiveness of boron-containing ores in Liaoning province of China against gamma rays and thermal neutrons

Meng-Ge Dong[1] · Xiang-Xin Xue[1] · V. P. Singh[2] · He Yang[1] · Zhe-Fu Li[3] · M. I. Sayyed[4]

Received: 16 March 2017 / Revised: 4 May 2017 / Accepted: 2 June 2017 / Published online: 19 March 2018

Abstract In this study, the mass attenuation coefficient of boron-containing ores in the Liaoning province of China was calculated using WinXCOM software to investigate the shielding effectiveness of these ores against gamma rays. The mass attenuation coefficients were also calculated using MCNP-4B code and compared with WinXCOM results; consequently, a good consistency between the results of WinXCOM and MCNP-4B was observed. Furthermore, the G-P fitting method was used to evaluate the values of exposure buildup factor (EBF) in the energy range of 0.015–15 MeV up to 40 mean free paths. Among the selected ores, boron-bearing iron concentrate ore (M3) was determined to be the best gamma ray shielding ore owing to its higher values of mass attenuation coefficient and equivalent atomic number and lower value of EBF. Moreover, American Evaluated Nuclear Data File (ENDF/B-VII) was used to analyze the shielding effectiveness against thermal neutrons. It was determined that Szaibelyite (M2) is the best thermal neutron shielding material. This study would be useful for demonstrating the potential of boron-containing ores for applications in the field of nuclear engineering and technology.

Keywords Exposure buildup factors · Gamma ray · Neutron · Boron-containing ores · G-P fitting method

This work was supported by the National Natural Science Foundation of China (Nos. 51472048, 50774022) and the Key Laboratory Project of Liaoning Province Education Office (No. LZ 2014-022).

✉ Xiang-Xin Xue
xuexx@mail.neu.edu.cn

Meng-Ge Dong
mg_dong@163.com

1 Department of Resource and Environment, School of Metallurgy, Northeastern University, Shenyang 110819, China

2 Department of Physics, Karnatak University, Dharwad 580003, India

3 Shanghai Institute of Applied Physics, Shanghai 201800, China

4 Physics Department, University of Tabuk, Tabuk, Saudi Arabia

1 Introduction

China is rich in boron resources with its boron reserves ranking fourth after Turkey, USA, and Russia. Ludwigite and Szaibelyite are the main boron-containing ores in the Liaoning province of China, especially Ludwigite, which is abundant, geographically ubiquitous, and potentially cheap. Moreover, the second or third boron-containing ores would be produced in the process of utilization of Ludwigite, such as boron-bearing iron concentrate ore, boron concentrate, boron-rich slag, and boron mud. Boron-containing ores are widely used in the industrial and agricultural sectors. Approximately 50 boron-containing products can be manufactured. For example, these ores can be used as the raw material to produce borax, boric acid, and mineral materials [1–7]. Furthermore, boron exhibits good shielding performance against neutrons, especially thermal neutrons [8]. Hence, Li et al. [5–7] verified that the composite material of boron-containing ores has excellent shielding properties against neutrons and gamma rays. Furthermore, the experiment results demonstrated that boron-containing ores have vast potential in the field of nuclear engineering and technology; for example, the composite materials of boron-containing ores can be used as coating shielding materials or

Table 1 Composition of boron-containing ores

Elements	Ludwigite (M1)	Szaibelyite (M2)	Boron-bearing iron concentrate ore (M3)	Boron concentrate (M4)	Boron-rich slag (M5)	Boron mud (M6)
B	2.056	5.065	1.846	4.641	3.65	1.053
O	41.979	47.502	34.312	47.883	42.097	49.763
C	–	–	5.802	–	7.364	5.887
Na	–	–	–	0.089	–	1.881
Mg	22.57	31.807	13.407	25.689	21.068	24.116
Al	0.658	0.455	–	0.693	3.727	0.747
Si	9.754	12.066	3.849	12.067	10.763	10.512
S	0.92	–	1.217	0.865	–	–
Ca	–	2.004	–	0.571	10.541	0.766
Fe	22.063	1.101	39.567	7.502	0.79	5.275

biological shields to repair the structure and cracks in the process of preparation of concrete used in nuclear applications. Nevertheless, the shielding effectiveness of composite materials of boron-containing ores against neutrons and gamma rays has not been studied yet, and therefore, it is the key focus of this paper. Singh and Badiger [9] and Singh et al. [10] studied the shielding effectiveness of alloys, boron-containing materials, and glasses against gamma rays using the mass attenuation coefficient, exposure buildup factor (EBF), and removal cross section for fast neutrons. Kurudirek [11] studied the radiation shielding for different types of shielding concretes, lead base and non-lead base glass systems for some shielding concretes and glass systems in the energy region of 10 keV–1 GeV. Sayyed [12] and Sayyed et al. [13] calculated the values of mass attenuation coefficient and EBF for polymers and glasses to analyze their shielding properties.

It is well known that Beer–Lambert law ($I = I_0 e^{-\mu d}$) can be used to calculate the shielding properties of narrow gamma rays passing through a material; however, the formula for wide beam gamma rays requires a correction factor, EBF, which is expressed as $I = BI_0 e^{-\mu d}$ [14, 15]. EBF is employed in attenuation studies to have a deeper understanding of the gamma ray shielding effectiveness of a shielding material [16]. The ANSI/ANS-6.4.3-1991 Standard, Gamma-Ray Attenuation Coefficients and Buildup Factors for Engineering Materials, was reported to calculate the EBF of shielding materials [17]. The standard covers the values of EBFs for 23 elements in the energy range of 0.015–15 MeV from the penetration depths of 0.5–40 mfp. Furthermore, the G-P fitting method was developed to calculate EBFs consistent with the standard, with uncertainty $< 5\%$ [18, 19]. Moreover, ENDF/B-VII contains a comprehensive neutron cross section of elements, and it is used widely in analyzing neutron shielding properties [8, 20, 21].

Thus, mass attenuation coefficient, EBFs, and thermal neutron removal cross section are employed to study the shielding effectiveness of boron-containing ores in the Liaoning province of China. The study will evaluate the shielding effectiveness to reveal the potential of the boron-containing ores in the Liaoning province of China for applications in the field of nuclear engineering and technology. Moreover, this work will extend the utilization method of boron-containing ores.

2 Materials and methods

2.1 Material

The raw materials used in this work were Ludwigite (M1, 3.09 g/cm^3), Szaibelyite (M2, 2.58 g/cm^3), boron-bearing iron concentrate ore (M3, 3.95 g/cm^3), boron concentrate (M4, 2.69 g/cm^3), boron-rich slag (M5, 2.97 g/cm^3), and boron mud (M6, 2.51 g/cm^3). Furthermore, these boron-containing ores were purchased from Fengcheng Iron and Steel Group Co. Ltd., China. Table 1 lists the composition and densities of six boron-containing ores.

2.2 Methods

2.2.1 Exposure buildup factor (EBF) of boron-containing ores

In order to calculate the EBF, the G-P fitting parameters were obtained from the equivalent atomic number (Z_{eq}) using a logarithmic interpolation method. The calculations are illustrated step by step as follows:

1. Calculation of equivalent atomic number (Z_{eq});
2. Calculation of parameters for the G-P fitting method;
3. Calculation of EBFs.

The atomic number of a single element is denoted by Z, whereas ore samples have an equivalent atomic number

(Z_{eq}), because the gamma ray partial interaction processes with the material depend on the energy. Thus, Z_{eq} is an energy-dependent parameter. Using the WinXCOM [22, 23] program, the total mass attenuation coefficient of the selected boron-containing ores in the Liaoning province of China and Compton partial mass attenuation coefficient for the elements from $Z = 4$ to $Z = 50$ were obtained in the energy range of 0.015–15 MeV. The equivalent atomic number is calculated by matching the ratio of Compton partial mass attenuation coefficient to the total mass attenuation coefficient of the selected ores with an identical ratio for a single element at the same energy. The following formula is used to interpolate Z_{eq} [24, 25]:

$$Z_{eq} = \frac{Z_1(\log R_2 - \log R) + Z_2(\log R - \log R_1)}{(\log R_2 - \log R_1)}, \quad (1)$$

where Z_1 and Z_2 are the atomic numbers of elements corresponding to the ratios R_1 and R_2, respectively, and R is the aforementioned ratio of the boron-containing ores at a specific energy. For example, considering that the ratio $(\mu/\rho)_{Compton}/(\mu/\rho)_{total}$ of boron-bearing iron concentrate ore (M3) at the energy of 0.015 MeV is 0.0052, which lies between $R_1 = (\mu/\rho)_{Compton}/(\mu/\rho)_{total} = 0.0057$ for $Z_1 = 18$ and $R_2 = (\mu/\rho)_{Compton}/(\mu/\rho)_{total} = 0.0048$ for $Z_2 = 19$, using Eq. (1), $Z_{eq} = 18.53$ is calculated. The G-P fitting parameters are calculated similarly using a logarithmic interpolation method for Z_{eq}. The change in Z_{eq} for the selected boron-containing ores with the incident photon energy is presented in Fig. 3.

As the second step, to evaluate the G-P fitting parameters (a, b, c, X_k, and d), a similar interpolation procedure was adopted as in the case of Z_{eq}. The G-P fitting parameters for the elements were obtained from the standard reference database released by the American National Standards ANSI/ANS-6.4.3 [17]. American Nuclear Society (ANSI/ANS-6.4.3, 1991) used the G-P fitting method and provided EBF data for 23 elements, one compound, and two mixtures, e.g., water, air, and concrete at 25 standard energies in the energy range of 0.015–15.0 MeV with a suitable interval up to the penetration depth of 40 mfp.

The G-P fitting parameters of the selected boron-containing ores were interpolated according to the following equation [24, 25]:

$$P = \frac{P_1(\log Z_2 - \log Z_{eq}) + P_2(\log Z_{eq} - \log Z_1)}{(\log Z_2 - \log Z_1)}, \quad (2)$$

where P_1 and P_2 are the values of the G-P fitting parameters at a particular energy, corresponding to the atomic numbers Z_1 and Z_2, respectively.

Finally, the calculated G-P fitting parameters were used to calculate the EBF of the selected boron-containing ores as follows [24, 25]:

$$B(E,x) = 1 + \frac{b-1}{K-1}(K^x - 1), \quad \text{for } K \neq 1$$
$$B(E,x) = 1 + (b-1)x, \quad \text{for } K = 1 \quad (3)$$

$$K(E,x) = cx^a + d\frac{\tanh(x/X_k - 2) - \tanh(-2)}{1 - \tanh(-2)}, \quad \text{for } x \leq 40 \text{ mfp} \quad (4)$$

where E is the incident photon energy, a, b, c, X_k, and d are the G-P fitting parameters, x is the penetration depth in the mean free path, and K is the photon dose multiplication. The mean free path (mfp) is the average distance between two successive interactions of photons wherein the intensity of the incident photon beam is reduced by a factor of $1/e$.

2.2.2 Macro-cross section of boron-containing ores for thermal neutrons

ENDF/B-VII (American Evaluated Nuclear Data File) [20] provided the micro-cross section of all the elements for neutrons at different energies and up to the neutron energy of 20 MeV. Moreover, boron is well known for its excellent shielding property against thermal neutrons [8]. Hence, the macro-cross section of boron-containing ores for shielding against thermal neutrons was calculated using Eq. (5) as follows [7]:

$$\sum E = N_A \rho \sum_i \frac{\omega_i}{M_i}\left(\sum E\right)_i, \quad (5)$$

where $\sum E$ (cm^{-1}) is the macro-cross section, N_A is the Avogadro constant, ρ is the density of the boron-containing

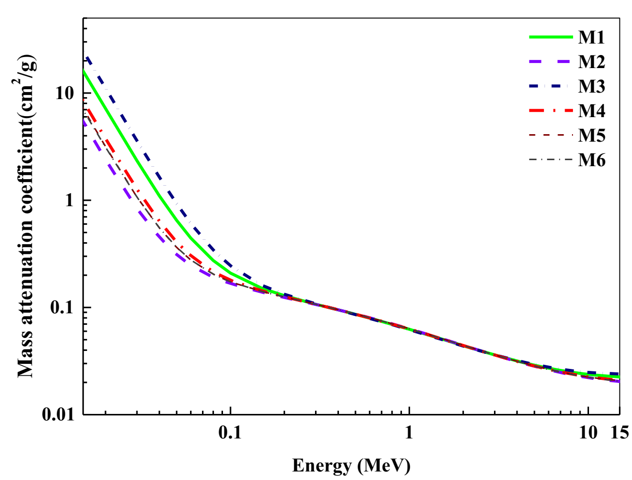

Fig. 1 (Color online) Total mass attenuation coefficient of boron-containing ores in the energy range of 0.015–15 MeV

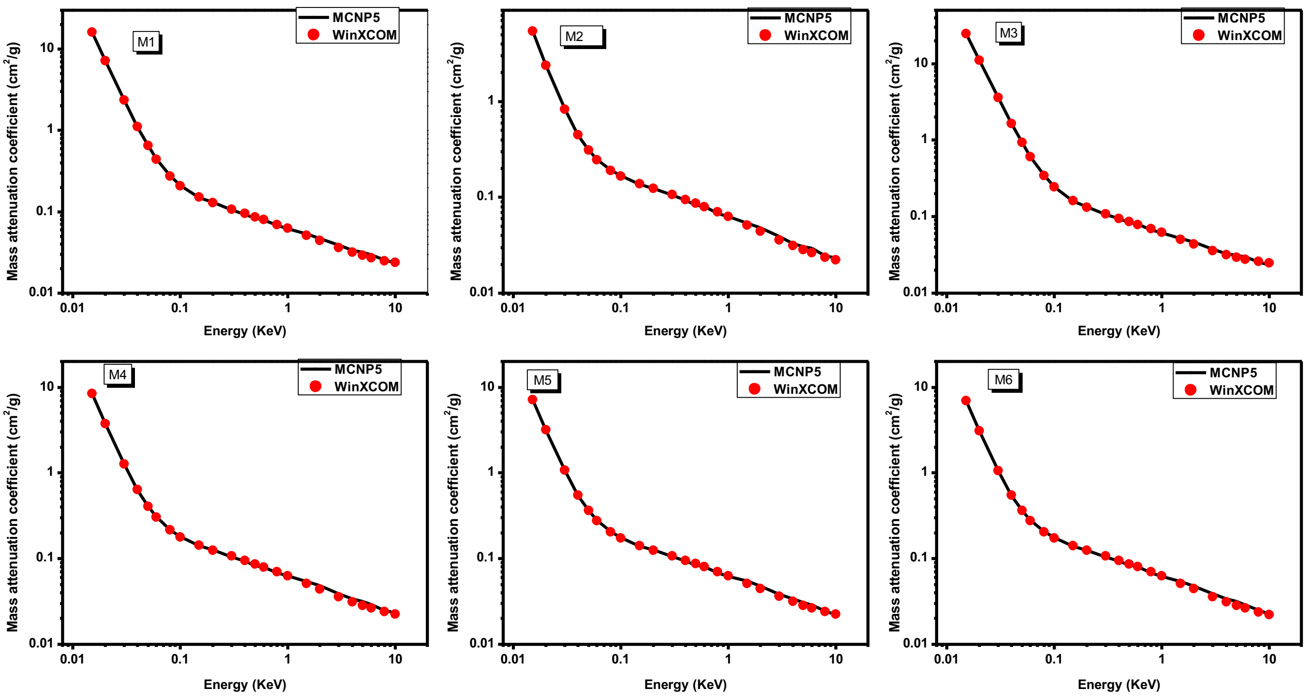

Fig. 2 (Color online) Comparison between the calculated values of mass attenuation coefficients of MCNP-4B and WinXCOM versus photon energy for the boron-containing ores

ore, and ω_i, M_i, and $(\sum E)_i$ are the mass fraction, molar mass, and macro-cross section of *i*th element, respectively.

3 Results and discussion

3.1 Shielding effectiveness of boron-containing ores against gamma rays

In this work, we evaluated the radiation attenuation properties of boron-containing ores by using MCNP-4B Monte Carlo code to calculate the mass attenuation coefficient for M1–M6 samples. The validation of MCNP-4B code was performed by comparing the results with standard WinXCOM data.

The mass attenuation coefficients (μ/ρ) of the boron-containing ores calculated using WinXCOM in the photon energy range of 0.015–15 MeV are shown in Fig. 1. Furthermore, the calculated values of μ/ρ are shown in Fig. 2 together with MCNP-4B results. The variation of Z_{eq} of boron-containing ores for the photon energy range of 0.015–15 MeV is shown in Fig. 3. Furthermore, the variation in the EBFs of boron-containing ores is shown in Fig. 4 (M1–M6) at constant penetration depth (0.5, 5, 10, 20, and 40 mfp). Furthermore, Fig. 5 shows the EBFs as a function of penetration depth at constant photon energy (0.015, 0.15, 1.5, and 15 MeV).

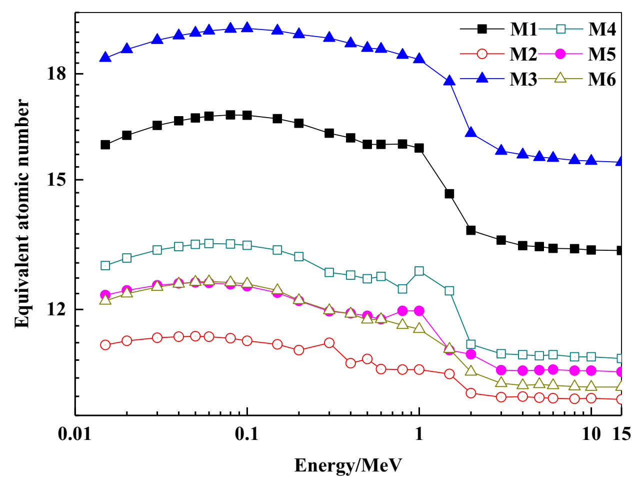

Fig. 3 (Color online) Variation of Z_{eq} of boron-containing ores in the energy range of 0.015–15 MeV

From Fig. 1, it can be observed that the mass attenuation coefficients of the selected boron-containing ores decrease rapidly in the energy range of 0.015–0.1 MeV, slowly decrease in the energy range of 0.1–10 MeV, and again increase in the energy range of 10–15 MeV. The variation in the values of mass attenuation coefficients with energy can be explained by partial photon interaction processes (photoelectric absorption, Compton scattering, and pair production) as the interaction cross section depends on photon energy and atomic number. The interaction cross section is directly proportional to the atomic number (Z^4)

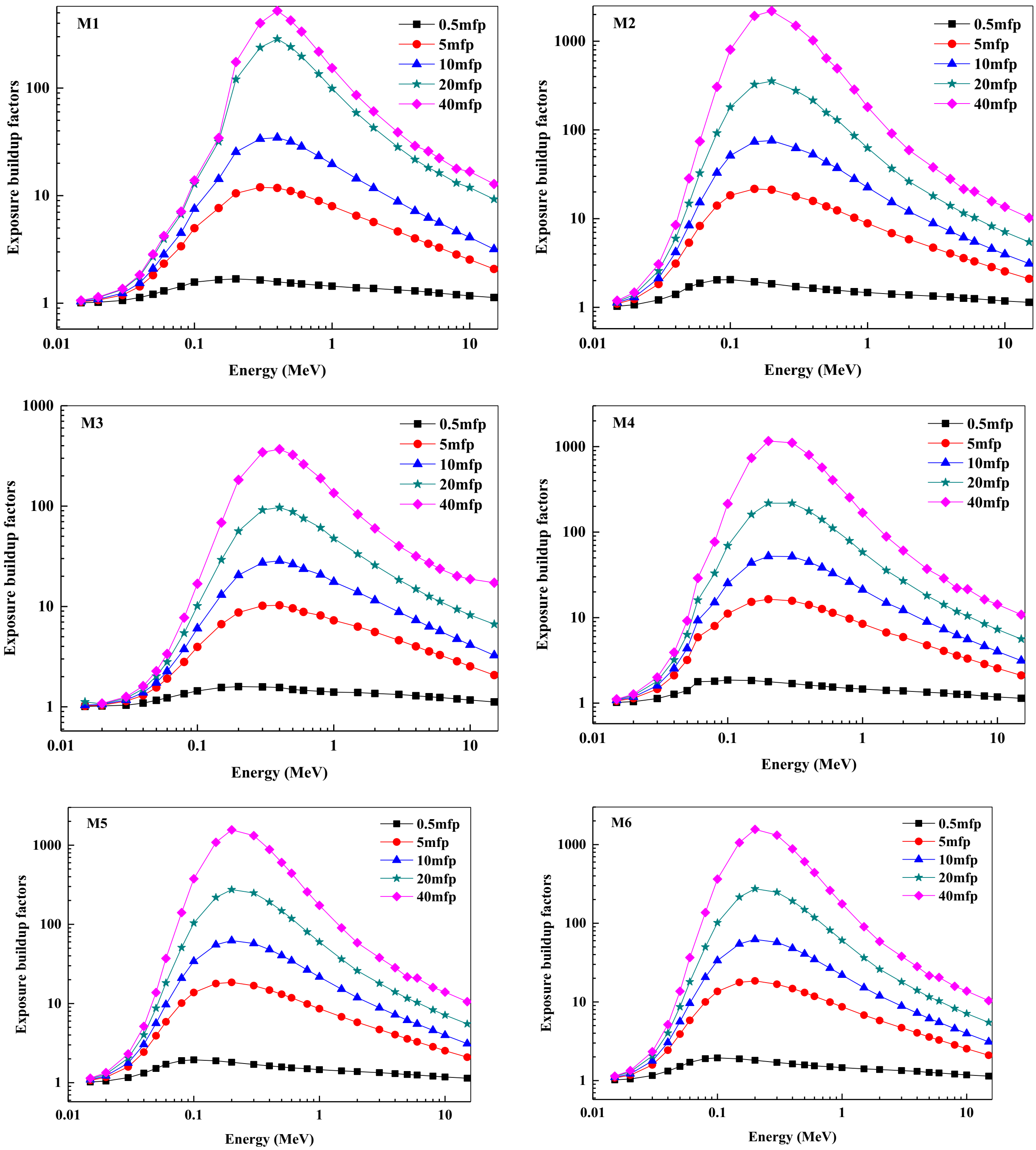

Fig. 4 (Color online) Variation of EBFs of boron-containing ores (M1–M6)

for photoelectric absorption in the energy region of 0.015–0.1 MeV; therefore, the values of μ/ρ for the boron-containing ores decrease rapidly. In the Compton scattering region (0.1–10 MeV), the interaction cross section is dependent on Z, whereas the cross section is directly proportional to Z^2 for pair production (10–15 MeV) [26]. According to Fig. 1, it can be observed that the value of μ/ρ of boron-bearing iron concentrate ore (M3) is the highest among the selected ores. It can be concluded that M3 is the best boron-containing ore for gamma ray shielding in the energy region of 0.015–0.1 MeV. From Fig. 2, it can be observed that the values of μ/ρ simulated using MCNP-4B

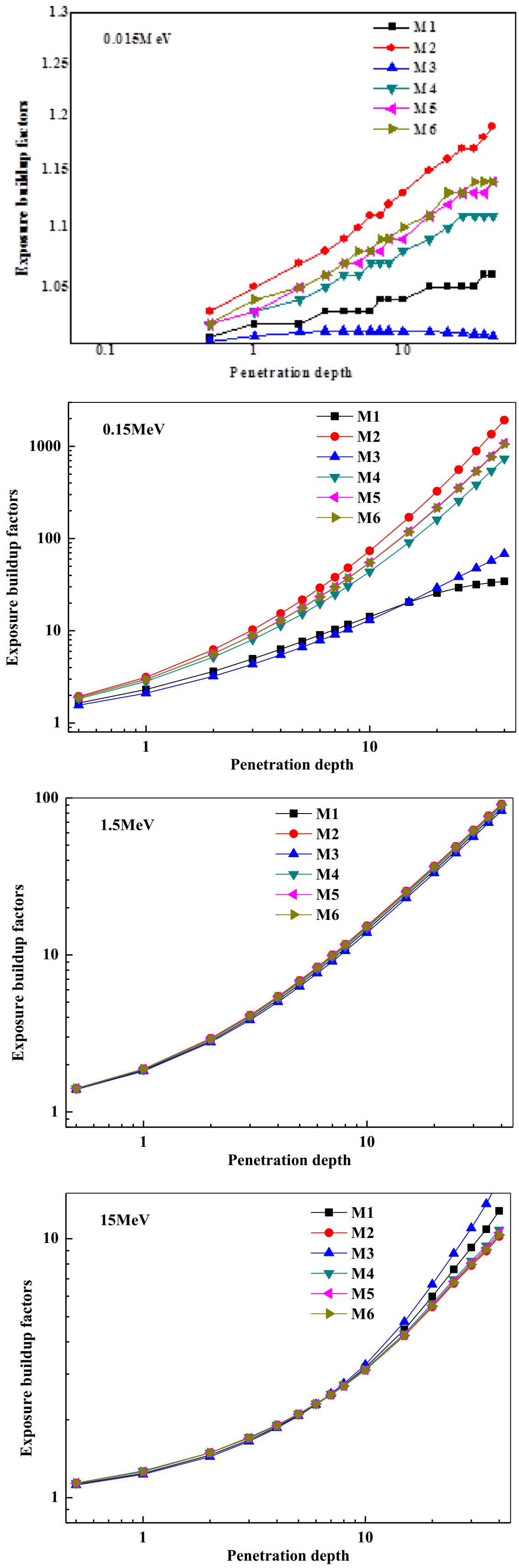

Fig. 5 (Color online) Variation of EBF of boron-containing ores with the penetration depth (0.015, 0.15, 1.5, 15 MeV)

for all the samples (M1–M6) are consistent with the theoretical estimation using WinXCOM.

From Fig. 3, it can be observed that the values of Z_{eq} of the boron-containing ores increase slightly and subsequently decrease with further increase in the incident photon energy up to 4 MeV. However, the values of Z_{eq} of all the boron-containing ores are approximately the same in the energy range of 4–15 MeV.

The variation of EBF of the boron-containing ores with the photon energy (0.015–15 MeV) is shown in Fig. 4. From Fig. 4, it can be observed that the EBF increases up to a maximum value (at 0.2 MeV) and decreases thereafter. The variation of EBF with the photon energy can be explained by the photon interaction process (similar to the mass attenuation coefficient). The EBF values of the boron-containing ores are minimal at low energy owing to the dominance of photoelectric effect. With the increase in the incident photon energy, EBF increases owing to multiple scattering as Compton scattering dominates. In the high-energy region, pair production takes over the Compton scattering process, resulting in the reduction of EBF to a minimum value. Notably, the boron-containing ore with the highest Z_{eq} (i.e., M3) achieves the minimum values of EBF. From Table 1, the content of Fe in M3 is 39.567%. This high content of Fe leads to the highest equivalent atomic number (Z_{eq}) of M3 as shown in Fig. 3, such that M3 has the lowest EBFs. Hence, it is the best boron-containing ore for gamma ray shielding.

The variation of EBFs of the boron-containing ores with the penetration depth is shown in Fig. 5. It can be observed that the EBF values of boron-containing ores increase with the increase in the penetration depth and they are the lowest for the penetration depth of 1 mfp and highest for

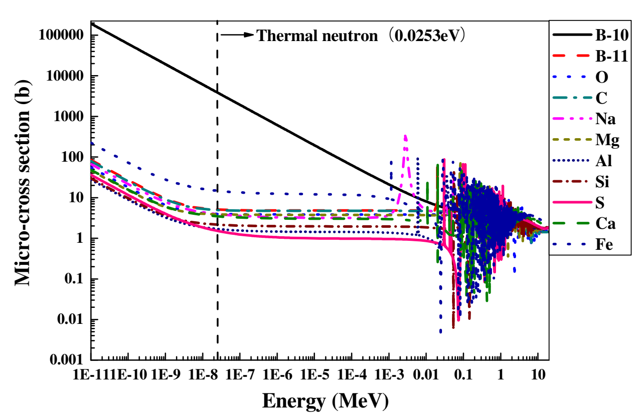

Fig. 6 Micro-cross section of elements contained in boron-containing ores for thermal neutrons

Table 2 Micro-cross section of elements contained in boron-containing ores for thermal neutrons

Element	B-10	B-11	O	C	Na	Mg	Al	Si	S	Ca	Fe
Micro-cross section (b)	3847.52	5.07	3.98	4.94	3.92	3.87	1.69	2.16	1.51	3.47	14.75

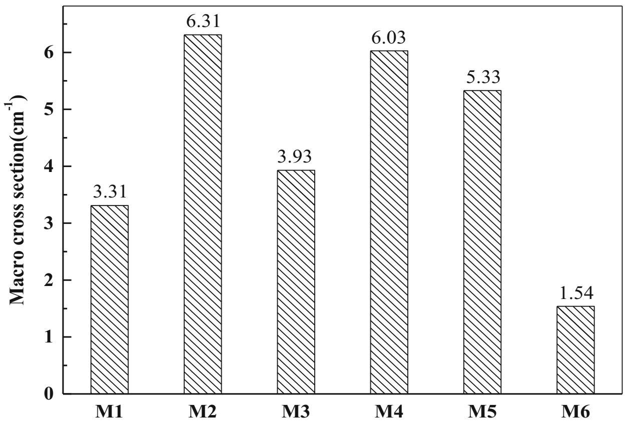

Fig. 7 Macro-cross section of boron-containing ores for thermal neutrons

the penetration depth of 40 mfp owing to multiple scattering events for large penetration depths. It can be observed that, at 0.015 MeV, the values of EBF of all the boron-containing ores are in the range of 1–1.2. Furthermore, at the photon energy of 1.5 MeV, the EBFs of all the ores are approximately the same. At the photon energy of 15 MeV, M3 shows the maximum value of EBF above the penetration depth of 10 mfp owing to pair production in the ores, which generates electron pairs. This trend reversal can be explained on the basis that, at this incident photon energy (i.e., 15 MeV), pair production is the dominant photon interaction process [27].

3.2 Macro-cross section for thermal neutrons

Figure 6 shows the data for the neutron micro-cross section of elements contained in the six boron-containing ores at the energy up to 20 MeV. The energy of thermal neutrons is chosen as 0.0253 eV [28–30] in this study as shown in Fig. 6. Moreover, the contents of B-10 isotope and B-11 isotope are calculated according to the natural boron content [8]. Table 2 presents the specific data for thermal neutrons of the elements contained in six boron-containing ores. From Fig. 6 and Table 2, the micro-cross section of B-10 is approximately 3847.52b and significantly more than that of the other elements; the micro-cross section of Fe is significantly less than that of B-10, but slightly more than that of the other elements. Moreover, the micro-cross sections for thermal neutrons of the other elements are approximately the same.

Figure 7 shows the macro-cross section of all the boron-containing ores for thermal neutrons. M2 is observed to have the highest macro-cross section, and the lowest is observed for M6. Compared with the B element content of ores, it can be concluded that the more the B element content of ores, the better the shielding properties of boron-containing ores. However, M1 and M3 are the opposite, because the B content of these two ores is approximately the same, but the Fe content of these two ores is quite different, i.e., approximately 22% in M1 and 40% in M3. However, the micro-cross section of the Fe element is slightly higher than that of the other elements and it leads to the difference between removal cross sections of the two ores. Nevertheless, M2 is the best ore for thermal neutron shielding.

4 Conclusion

In this study, we first studied the shielding effectiveness of boron-containing ores in the Liaoning province of China against gamma rays and thermal neutrons, which has potential applications in the field of nuclear engineering and technology. Furthermore, we calculated the mass attenuation coefficient and EBF. The EBF values of boron-containing ores were calculated using the G-P fitting formula in the energy range of 0.015–15 MeV from 0.5 to 40 mfp. ENDF/B-VII provided the micro-cross section of each element contained in boron-containing ores to analyze the shielding effectiveness against thermal neutrons. Among the studied ores, boron-bearing iron concentrate ore (M3) and Szaibelyite (M2) showed superior shielding properties against gamma rays and thermal neutrons, respectively. This study would be useful for demonstrating the potential of boron-containing ores for applications in the field of nuclear engineering and technology.

References

1. J. An, X.X. Xue, Life cycle environmental impact assessment of borax and boric acid production in China. J. Clean. Prod. **66**, 121–127 (2014). https://doi.org/10.1016/j.jclepro.2013.10.020
2. G. Wang, Q.G. Xue, J.S. Wang, Effect of Na_2CO_3 on reduction and melting separation of Ludwigite/coal composite pellet and property of boron-rich slag. Trans. Nonferrous Met. Soc. **26**,

282–293 (2016). https://doi.org/10.1016/S1003-6326(16)64116-X

3. G. Wang, Y.G. Ding, J.S. Wang et al., Effect of carbon species on the reduction and melting behavior of boron-bearing iron concentrate/carbon composite pellets. Int. J. Min. Met. Mater. **20**, 522–528 (2013). https://doi.org/10.1007/s12613-013-0760-1
4. X. Ma, H. Ma, X. Jiang et al., Preparation of magnesium hydroxide nanoflowers from boron mud via anti-drop precipitation method. Mater. Res. Bull. **56**, 113–118 (2014). https://doi.org/10.1016/j.materresbull.2014.04.021
5. Z.F. Li, X.X. Xue, T. Jiang et al., Study on the properties of boron containing ores/epoxy composites for slow neutron shielding. Adv. Mater. Res. **201–203**, 2767–2771 (2011). https://doi.org/10.4028/www.scientific.net/AMR.201-203.2767
6. Z.F. Li, X.X. Xue, P.N. Duan et al., Preparation and thermal/fast neutron shielding properties of novel boron containing ore composites. Mater. Sci. Forum **743–744**, 613–622 (2013). https://doi.org/10.4028/www.scientific.net/MSF.743-744.613
7. Z.F. Li, X.X. Xue, S.L. Liu et al., Effects of boron number per unit volume on the shielding properties of composites made with boron ores from China. Nucl. Sci. Tech. **23**, 344–348 (2012). https://doi.org/10.13538/j.1001-8042/nst.23.344-348
8. J.C. Khong, D. Daisenberger, G. Burca et al., Design and characterisation of metallic glassy alloys of high neutron shielding capability. Sci. Rep. **6**, 36998 (2016). https://doi.org/10.1038/srep36998
9. V.P. Singh, N.M. Badiger, γ-ray interaction characteristics for some boron containing materials. Vacuum **113**, 24–27 (2015). https://doi.org/10.1016/j.vacuum.2014.11.011
10. V.P. Singh, N.M. Badiger, N. Chanthima et al., Evaluation of gamma-ray exposure buildup factors and neutron shielding for bismuth borosilicate glasses. Radiat. Phys. Chem. **98**, 14–21 (2014). https://doi.org/10.1016/j.radphyschem.2013.12.029
11. M. Kurudirek, Radiation shielding and effective atomic number studies in different types of shielding concretes, lead base and non-lead base glass systems for total electron interaction: a comparative study. Nucl. Eng. Des. **280**, 440–448 (2014). https://doi.org/10.1016/j.nucengdes.2014.09.020
12. M.I. Sayyed, Bismuth modified shielding properties of zinc boro-tellurite glasses. J. Alloys Compd. **688**, 111–117 (2016). https://doi.org/10.1016/j.jallcom.2016.07.153
13. M.I. Sayyed, S.I. Quashu, Z.Y. Khattari, Radiation shielding competence of newly developed TeO_2-WO_3 glasses. J. Alloys Compd. (2016). https://doi.org/10.1016/j.jallcom.2016.11.160
14. M.I. Sayyed, Half value layer, mean free path and exposure buildup factor for tellurite glasses with different oxide compositions. J. Alloys Compd. **695**, 3191–3197 (2017). https://doi.org/10.1016/j.jallcom.2016.11.318
15. M. Kurudirek, D. Sardari, N. Khaledi et al., Investigation of X- and gamma ray photons buildup in some neutron shielding materials using GP fitting approximation. Ann. Nucl. Energy **53**, 485–491 (2013). https://doi.org/10.1016/j.anucene.2012.08.002
16. U. Fano, Gamma-ray attenuation. Part II—analysis of penetration. Minerva Med. **11**, 55–61 (1953)
17. ANSI/ANS-6.4.3, Gamma ray attenuation coefficient and buildup factors for engineering materials (1991)
18. Y. Harima, Y. Sakamoto, S. Tanka et al., Validity of geometric progression formula in approximating gamma ray buildup factor. Nucl. Sci. Eng. **94**, 24–25 (1986)
19. Y. Harima, An historical review and current status of buildup factor calculations and application. Radiat. Phys. Chem. **41**, 631–672 (1993). https://doi.org/10.1016/0969-806X(93)90317-N
20. M.B. Chadwick, M. Herman, P. Obložinský et al., ENDF/B-VII.1 nuclear data for science and technology: cross sections, covariances, fission product yields and decay data. Nucl. Data Sheets **112**, 2887–2996 (2011). https://doi.org/10.1016/j.nds.2011.11.002
21. G. Ilas, I.C. Gauld, G. Radulescu, Validation of new depletion capabilities and ENDF/B-VII data libraries in Scale. Ann. Nucl. Energy **46**, 43–55 (2012). https://doi.org/10.1016/j.anucene.2012.03.012
22. M.J. Berger, J.H. Hubbell, XCOM: photon cross sections database, Web Version 3.1. http://physics.nist.gov/xcom, National Institute of Standards and Technology, Gaithersburg, MD 20899, USA, 1987/99. Originally published as NBSIR 87-3597 "XCOM: Photon Cross Sections on a Personal Computer"
23. M.G. Dong, X.X. Xue, H. Yang et al., A novel comprehensive utilization of vanadium slag: as gamma ray shielding material. J. Hazard. Mater. **318**, 751–757 (2016). https://doi.org/10.1016/j.jhazmat.2016.06.012
24. M. Kurudirek, M. Aygun, S.Z. Erzeneoglu, Chemical composition, effective atomic number and electron density study of trommel sieve waste (TSW), Portland cement, lime, pointing and their admixtures with TSW in different proportions. App. Radiat. Isot. **68**, 1006–1011 (2010). https://doi.org/10.1016/j.apradiso.2009.12.039
25. S.M. Kulwinder, S.S. Gurdeep, Verification of some low-Z silicates as gamma-ray shielding materials. Ann. Nucl. Energy **40**, 241–252 (2012). https://doi.org/10.1016/j.anucene.2011.09.015
26. Y. Elmahroug, B. Tellili, C. Souga, Determination of total mass attenuation coefficients, effective atomic numbers and electron densities for different shielding materials. Ann. Nucl. Energy **75**, 268–274 (2015). https://doi.org/10.1016/j.anucene.2014.08.015
27. M.I. Sayyed, H. Elhouichet, Variation of energy absorption and exposure buildup factors with incident photon energy and penetration depth for boro-tellurite (B_2O_3–TeO_2) glasses. Radiat. Phys. Chem. **130**, 335–342 (2017). https://doi.org/10.1016/j.radphyschem.2016.09.019
28. H.S. Chen, W.X. Wang, Y.L. Li et al., The design, microstructure and tensile properties of B_4C particulate reinforced 6061Al neutron absorber composites. J. Alloys Compd. **632**, 23–29 (2015). https://doi.org/10.1016/j.jallcom.2015.01.048632:23-29
29. V.F. Sears, Neutron scattering lengths and cross sections. Neutron News. **3**, 26–37 (2006). https://doi.org/10.1080/10448639208218770
30. T. Özdemir, İ.K. Akbay, H. Uzun et al., Neutron shielding of EPDM rubber with boric acid: mechanical, thermal properties and neutron absorption tests. Prog. Nucl. Energy **89**, 102–109 (2016). https://doi.org/10.1016/j.pnucene.2016.02.007